Microstructure and mechanical properties of Al–xMg alloys processed by room temperature ECAP

Y.J. Chen [a,*], Y.C. Chai [b], H.J. Roven [a], S.S. Gireesh [a], Y.D. Yu [a], J. Hjelen [a]

[a] Department of Materials Science and Engineering, Norwegian University of Science and Technology, 7491 Trondheim, Norway
[b] National Engineering Research Center of Light Alloy Net Forming, Shanghai Jiao Tong University, Shanghai 200240, China

a b s t r a c t

Microstructure development and mechanical properties of Al–xMg alloys (x = 0, 1, 5–10 wt%), processed by ECAP at room temperature, have been investigated. The results show that the microstructures of Al–xMg alloys are refined by the interaction of shear bands and their increase in number during ECAP. The addition of magnesium to aluminum promotes the grain refinement. Misorientation increase induced by particles along grain boundaries is observed by using high resolution EBSD. As ECAP strain increases up to 4, the strength of Al–6 wt% Mg alloy increases progressively while the elongation decreases from 31.7% to 5.5%. A good combination of both strength and ductility has been obtained by annealed ECAP. The change in softening mechanism of the Al–6 wt% Mg alloy, processed by 6 passes of annealed ECAP, occurs in the range of 523–573 K.

Keywords:
Aluminum alloys
Electron backscatter diffraction (EBSD)
Equal channel angular pressing (ECAP)
Microstructure
Grain refinement
Mechanical properties

(1) Introduction

At present, the development of equal channel angular pressing (ECAP) has attracted much attention from the material scientists because of its ability to easily refine the grains of metals with accumulative strain [1]. The metals processed by ECAP normally present a very high strength due to their small grains and high dislocation density [2]. Many papers have reported the promising results of Al and its alloys processed by ECAP. In particular, fine grained Al–3 wt% Mg alloy with a mean grain size of 200 nm was obtained by ECAP at room temperature followed by cold rolling [3]. The grain size of Al–1.5 wt% Mg reached 280 nm and 230 nm after ECAP strain up to 8 and 13, respectively [4]. In general, the mean grain sizes of commercial aluminum-based alloys can be reduced into a submicrometer range by ECAP at room temperature [5].

However, processing of Al–xMg alloys containing more than 4 wt% Mg by ECAP is not so easy. It normally requires elevated temperature to reduce the possibility of cracking. Cracks have been found in a 5083 Al–Mg alloy processed by ECAP at room temperature [6]. The grain size may grow during ECAP and between ECAP passes when the materials are exposed at high temperature. Thus the grain size is normally larger than the ECAP at low temperature [7]. In addition, electron backscatter diffraction (EBSD) investigation of Al–xMg alloys after ECAP is very difficult due to the experienced low intensity of the Kikuchi diffraction patterns caused by strain and magnesium addition, especially for high magnesium content (≥5 wt%). As a result, there are few publications reporting the EBSD investigations of Al–xMg alloys (≥5 wt%) after ECAP. The aim of the present paper is to process the Al–xMg alloys by ECAP at room temperature and to investigate the microstructure development and the improvement of mechanical properties.

(2) Experimental procedure

In this study the Al–xMg alloys (x = 0, 1, 5–10 wt%) were received in the as-cast condition. The chemical composition of all alloys used in this study is shown in Table 1. In order to effectively dissolve Mg-rich particles formed during casting and to obtain a nearly homogenous solid solution distribution of Mg, Al–(0, 1) wt% Mg alloys, Al–(5–7) wt% Mg alloys, and Al–(8–10) wt% Mg alloys were homogenized for 3 h at 853 K, 773 K and 753 K, respectively. The grain sizes calculated by polarized optical microscopy (POM) are 660 μm, 960 μm, 61 μm, 60 μm, 116 μm and 84 μm for the homogenized Al–xMg alloys (x = 0, 1, 5–7 and 10 wt%), respectively. ECAP was performed via route Bc at room temperature on 100 mm × 19.5 mm × 19.5 mm bars with an L-shaped split-die with $\phi = 90°$ and $= 20.6°$, which leads to an imposed strain of about 1 per pass [8]. Pairs of samples were pressed continuously, with the second sample passing through the angle in the die forcing the

* Corresponding author at: Alfred Getz vei 2B, No-7491 Trondheim, Norway. Tel.: +47 73594921; fax: +47 73590203.
E-mail address: happywinner01@gmail.com (Y.J. Chen).

Table 1
Chemical composition of Al–xMg alloys used in udy.

Alloys	Mg	Fe	Si	Ti
Al–0 wt% Mg	0.00087	0.0581	0.0428	0.02
Al–1 wt% Mg	0.971	0.0722	0.0482	0.00
Al–5 wt% Mg	5.047	0.0569	0.0526	0.00
Al–6 wt% Mg	5.983	0.0579	0.0532	0.00
Al–7 wt% Mg	7.056	0.0654	0.0560	0.00
Al–8 wt% Mg	7.991	0.062	0.0574	0.00
Al–9 wt% Mg	9.048	0.056	0.0584	0.00
Al–10 wt% Mg	9.988	0.0585	0.0601	0.00

first sample out and the latter then being inserted immediately into the top channel of the die [9]. The homogenized Al–xMg alloys (x = 0, 1, 5–10 wt%) were deformed up to 3 ECAP passes at room temperature. However, the Al–xMg samples with high Mg content (x = 5–10 wt%) after 3 ECAP passes have obvious cracks in the top surfaces. In order to avoid the cracking problem, the Al–6 wt% Mg samples are chosen to perform 'annealed ECAP'. Samples for 'annealed ECAP' were taken out from ECAP die to anneal at 523 K for 5 min and at 623 K for 10 min in an oven between the second and the third pass, and between the fourth and the fifth pass, respectively. The annealed ECAP shows that Al–6 wt% Mg samples can be deformed up to 6 passes without significant cracks.

After processing, the center of the longitudinal plane of the selected Al–xMg (x = 0, 1, 5–7 and 10 wt%) samples was prepared for microstructure investigations. The Al–xMg samples (x ≥ 5) for EBSD observation were annealed at a low temperature (473 K for 1 h) to improve the intensity of the Kikuchi patterns. Vickers microhardness was measured in the middle area of each sample using a load of 300 gf and a dwell time of 15 s.

Samples for the EBSD study were prepared by mechanical grinding, mechanical polishing and final equipment) with a solution containing 20 pct perchloric acid 80 pct ethanol, using a voltage of 20 V for 25 s at −30 °C. Finally, samples were cleaned with methanol. The EBSD analysis was formed in a Zeiss Ultra, 55 Limited Edition FEG-SEM equipped a Nordif EBSD UF-1000 detector and a TSL OIM EBSD 5.31 ware. Step size of 140 nm was chosen for all EBSD scans, except for investigating the particles. Specimens for transmission electron microscopy (TEM) observation were prepared by thinning down to 100 μm followed by a double jet polishing in a solution containing with an electrolyte of 33% nitric acid–methanol at −40 °C. The TEM investigations were performed with a JEOL-2010 with a LaB_6 filament.

(3) Results

- Microstructure development of Al–xMg alloys processed by 3 ECAP passes

The typical POM microstructures of Al–xMg alloys processed by 3 ECAP passes are shown in Fig. 1. It is apparent that the microstructures consist of arrays of shear bands in Fig. 1a–d. The direction of shear bands is typically parallel to the shear direction (Fig. 1a), which is consistent with the slip lines of the third pass through the die [10]. This indicates that the dominant shear bands (one example is given by 45° with horizon line in Fig. 1a) are caused by the third pass. The shear bands have been subdivided into several isolated structures by their mutual interaction during the third and earlier passes. These subdivided structures tend to evolve from parallelogram structures into long fiber structures with increasing magnesium content, as shown in Fig. 2a and d.

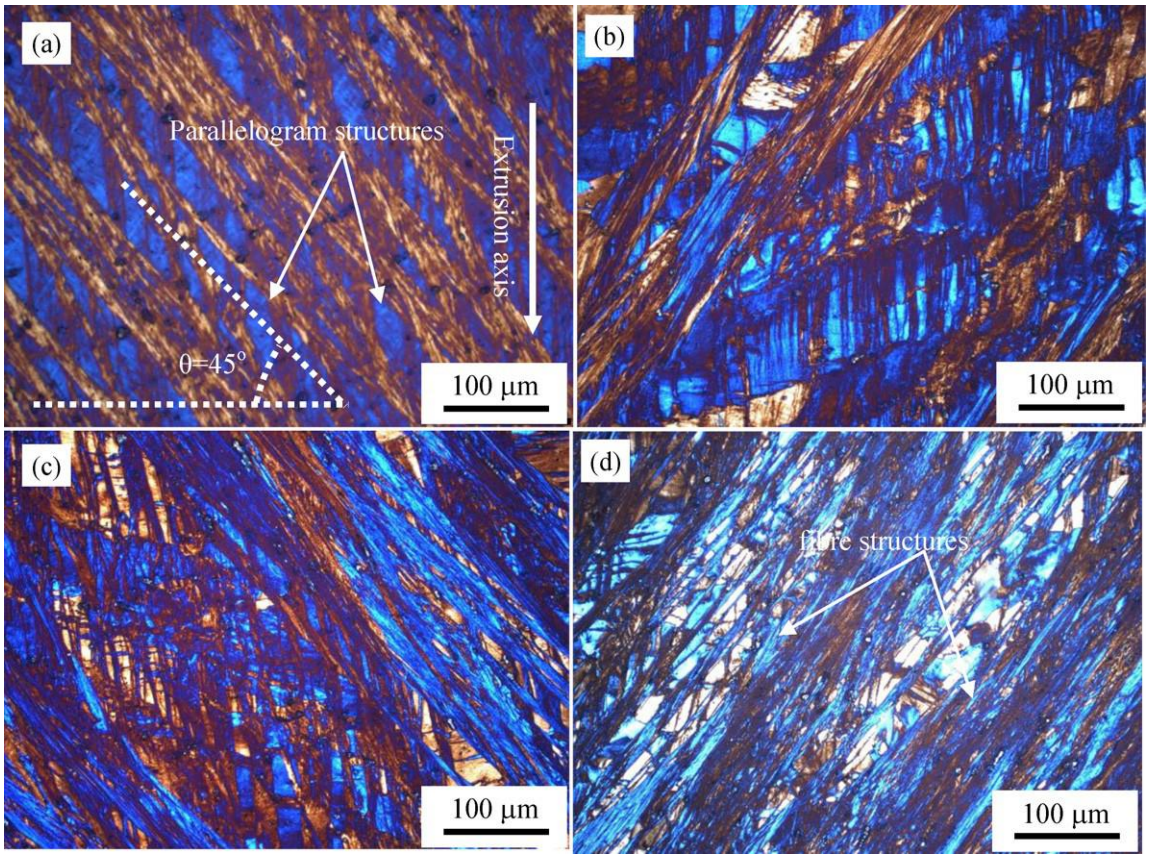

Fig. 1. Typical POM microstructures of Al–xMg alloys processed by 3 ECAP passes at room temperature and (a) 0, (b) 5, (c) 7, and (d) 10.

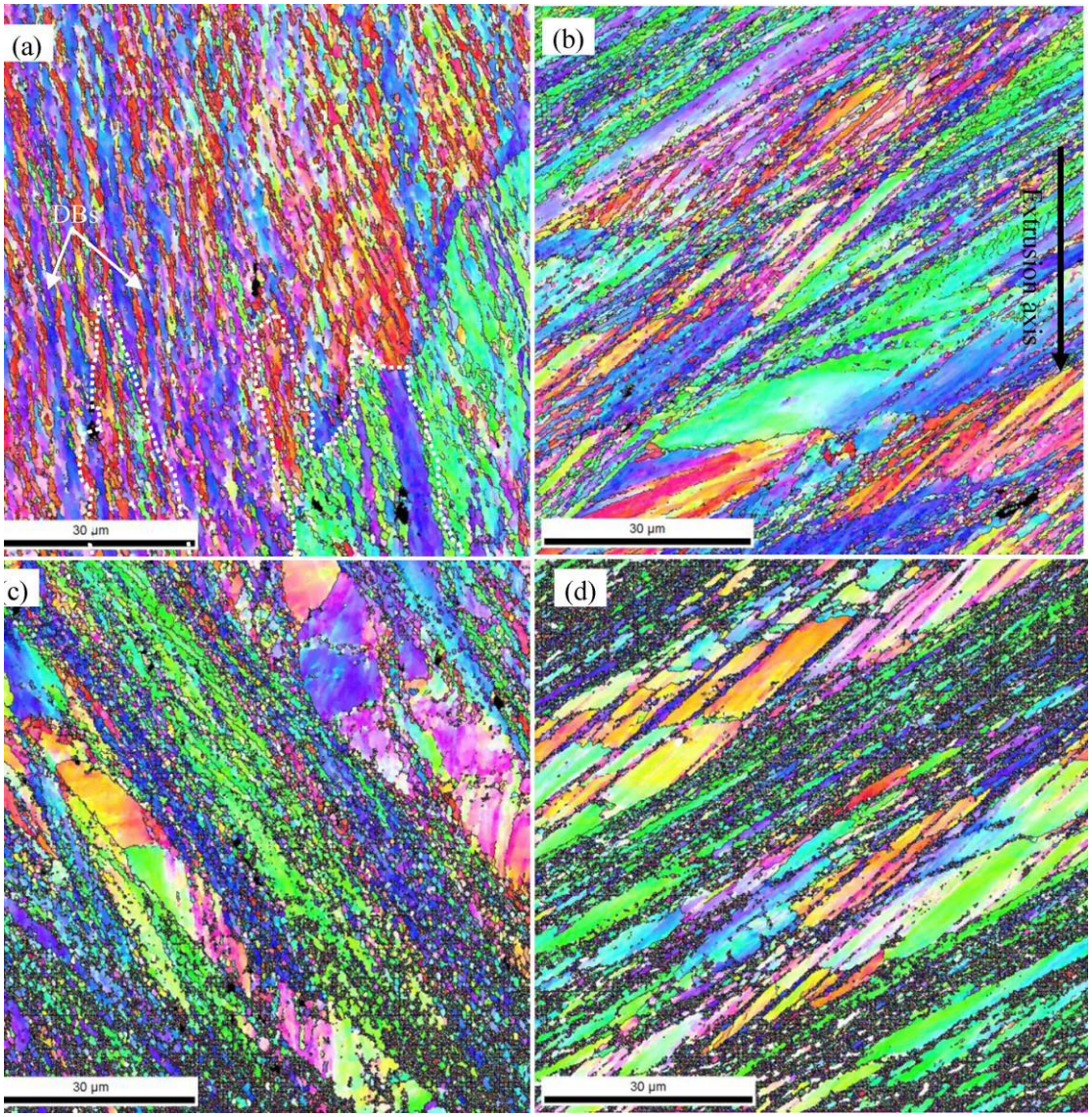

Fig. 2. Typical orientation maps (SEM-EBSD) of Al–xMg alloys processed by 3 ECAP passes at room temperature and (a) 0, (b) 5, (c) 7, and (d) 10.

Fig. 2 shows the typical orientation maps (SEM-EBSD) of Al–xMg alloys obtained after 3 ECAP passes at room temperature. High angle grain boundaries (HAGBs), with misorientations beyond 15°, are marked by black lines. Fig. 2a reveals a very heterogenous microstructure of pure Al obtained at 3 passes. The upper part of the original grain boundaries (marked with two white dashed lines) belongs to one coarse grain, which contains lots of parallel deformation bands (DBs). Although many new fine grains form in this coarse grain, the EBSD software treats it as one grain because its grain boundary is not completely closed by HAGBs. The elongated coarse grains/parallel DBs are the main features in Fig. 2b–d. The direction of the elongated coarse grains/DBs tends to be parallel to the shear direction, which is in agreement with the observation in Fig. 1. The width of the DBs and the grain size of fine grains tend to decrease with increasing magnesium content.

The grain size distributions (equivalent circle diameter, ECD) of each alloy calculated from Fig. 2 are shown in Fig. 3. It is clear that the distribution ranges of grain sizes tend to narrow gradually, regardless of the initial grain sizes, as magnesium content increases from 0 to 10% (Fig. 3a–d). The fraction of fine grain size tends to increase with increasing magnesium content (Fig. 3b–d), which suggests that the addition of magnesium stimulates the grain refinement.

Fig. 4 shows the misorientation map of Al–xMg alloys processed by ECAP at room temperature. The misorientation angle of pure Al after 3 ECAP passes decreases continuously from 1.5° to 65°. By contrast, the misorientation angles of Al–(5–10 wt%) Mg alloys present bimodal distribution. Comparing the curves at misorientation angles around 15° and 45°, it can be seen that increasing magnesium content decreases the fraction of low angle grain boundaries (LAGBs) and increases the fraction of HAGBs gradually.

Due to the optimum step size link with SEM magnification in EBSD [11], EBSD cannot reveal very fine grains (typically grain size less than 3 times of step size will be missed) and coarse grains together in a heterogenous microstructure. By contrast, TEM can provide detailed information for such fine grains. Fig. 5 shows the typical TEM microstructures of Al–xMg alloys processed by 3 ECAP passes. It can be seen that the microstructures of Al–xMg alloys after ECAP consist of arrays of elongated grains (subgrains). The width of the elongated grains (subgrains) tends to decrease with increasing magnesium content, as shown in Fig. 5a, c and d. Fig. 5b reveals that the deformation in grains is very heterogenous. It can be seen that

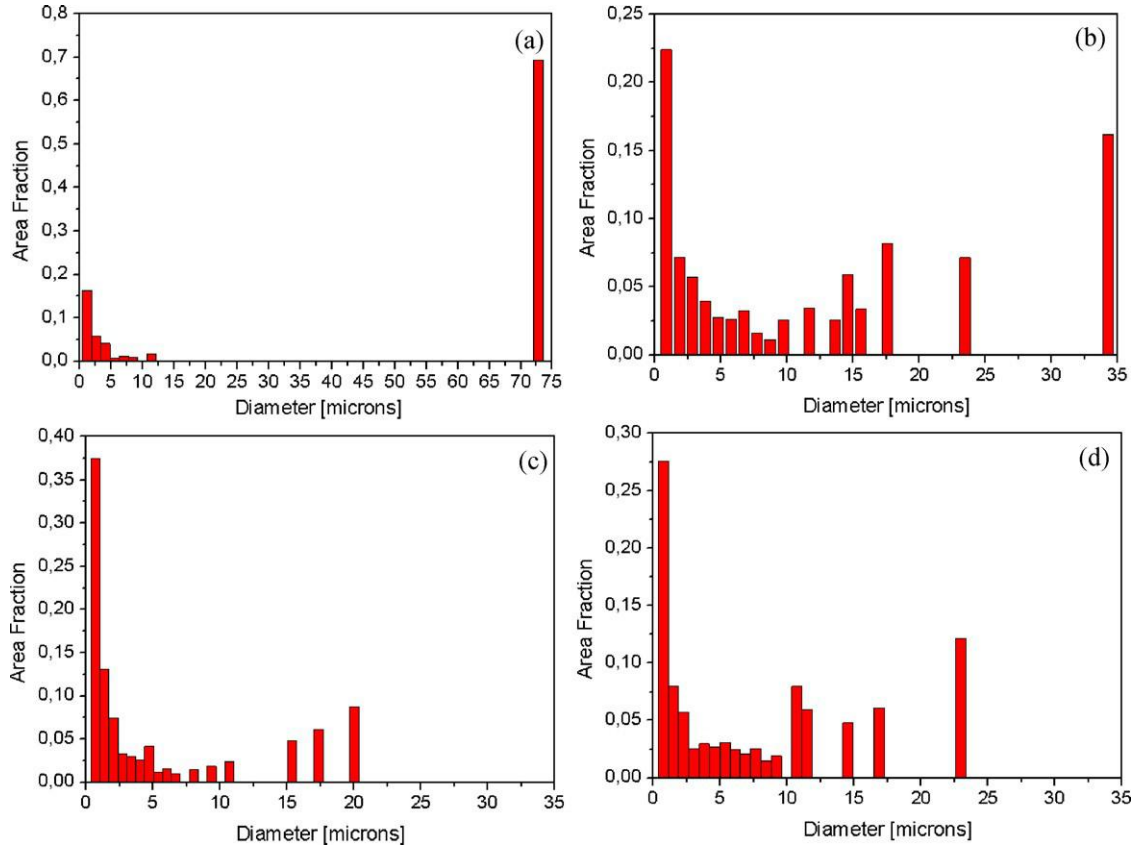

Fig. 3. Grain size distributions of Al–xMg alloys processed by 3 ECAP passes and (a) 0 (b) 5 (c) 7, and (d) 10, respectively.

the dislocation tangle zones (DTZs, marked in Fig. 5b) are produced around an original grain boundary. Some dislocation cells (DCs) are formed through a recovery process, i.e., the interaction, annihilation and rearrangement of dislocations [12]. It is apparent that more DCs could form to consume the interiors of the grains by increasing strain. The fine grains with mean grain size around 250 nm are formed in Al–7 wt% Mg alloy. The fine grains in Al–10 wt% Mg alloy are elongated and parallel to shear direction. The fine grain size is around 150 nm (Fig. 5d).

• Hardness development of Al–xMg alloys processed by 3 ECAP passes

Vickers hardness before and after ECAP measured at room temperature is plotted against the magnesium content of Al–xMg alloys in Fig. 6. It is seen that the hardness of Al–xMg alloys before ECAP increases almost linearly with increasing magnesium content. After 3 ECAP passes, the hardness of Al–xMg alloys increases sharply by a rough factor of 2. By Comparing the trend of the hardness curve in Al–xMg alloys (x = 0, 1 and 5 wt%) after ECAP, a small hardness drop can be observed in Al–(6–10 wt%) Mg after ECAP, which may be caused by the fact that obvious cracks appear in the top surfaces of these samples.

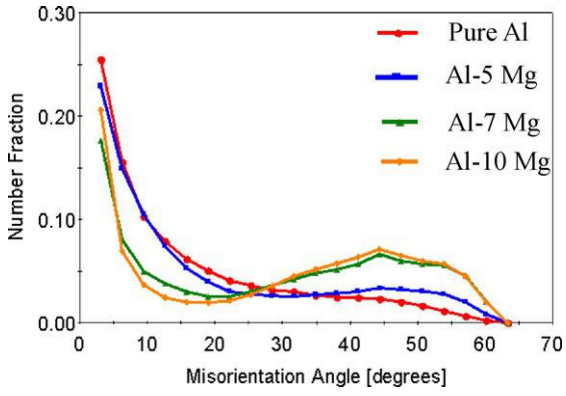

Fig. 4. Misorientation map of Al–xMg alloys processed by 3 ECAP passes at room temperature.

• Microstructure development of Al–6 wt% Mg alloy processed by annealed ECAP

Fig. 7 shows the typical POM microstructures of Al–6 wt% Mg alloy processed by annealed ECAP at room temperature. It is shown that the initial equiaxed grains are heavily elongated to form parallel shear bands after the first pass (Fig. 7a). With increasing ECAP strain (Fig. 7a–d), the width of shear bands tends to decrease and the number of shear bands increases gradually. It is apparent that the microstructure is refined by the interaction of shear bands and their increase in number. Fig. 7 shows the homogeneity of microstructure improves greatly with increasing strain.

• Mechanical properties of Al–6 wt% Mg alloy processed by annealed ECAP

Fig. 8 shows the tensile curves of Al–6 wt% Mg alloy processed by annealed ECAP. The yield strength (YS), ultimate tensile strength (UTS) and elongation are summarized in Table 2. It can be seen that both YS and UTS increase sharply after the first pass due to a lot of dislocations and refined grains introduced by ECAP. As ECAP strain increases up to 4, the strength (YS and UTS) increases progressively while the elongation decreases from 31.7% to 5.5%. The decrease in

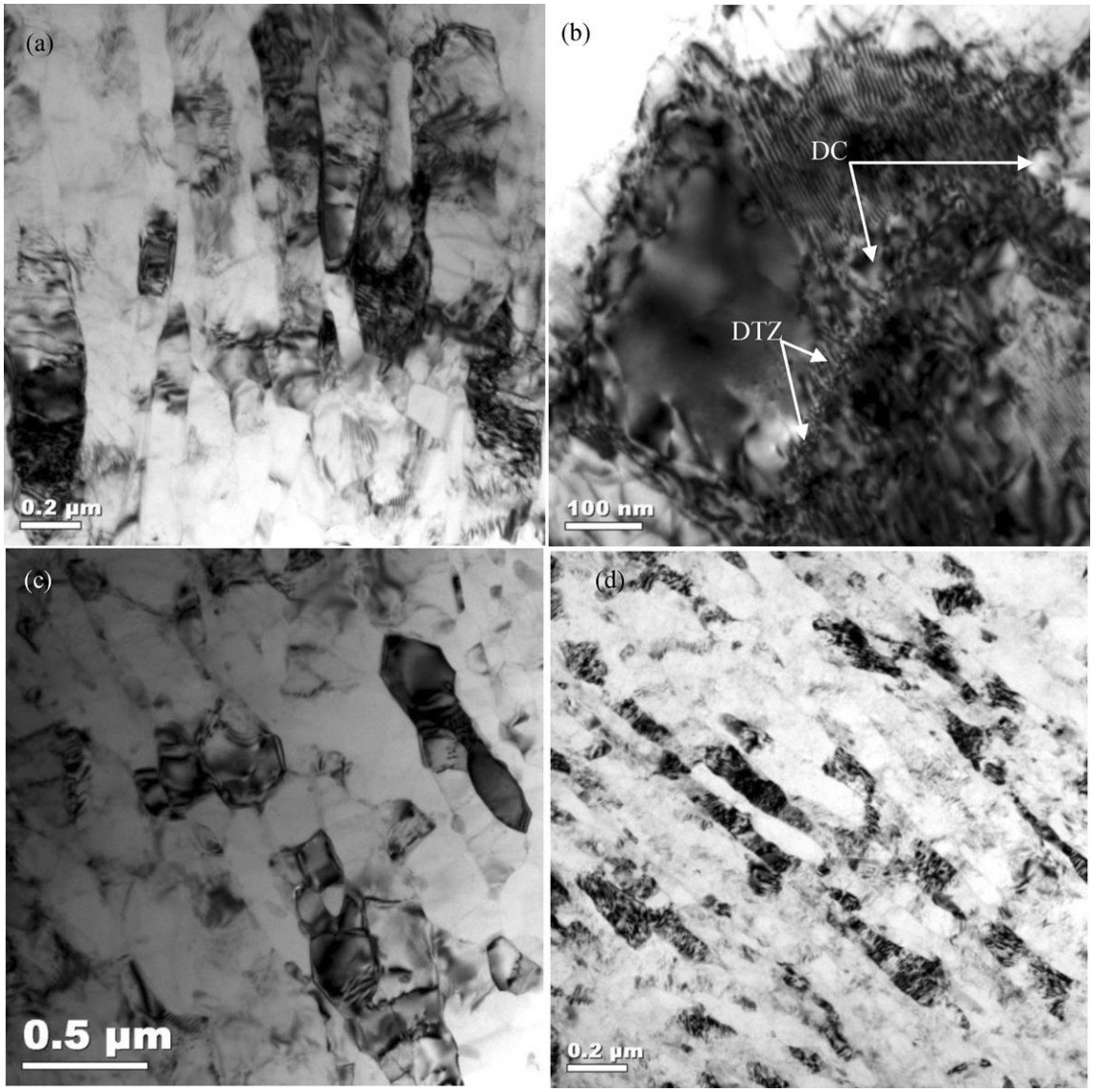

Fig. 5. Typical TEM microstructures of Al–xMg alloys processed by 3 ECAP passes and (a) Al–1 wt% Mg alloy, (b) Al–1 wt% Mg alloy at high magnification, (c) Al–7 wt% Mg alloy and (d) Al–10 wt% Mg.

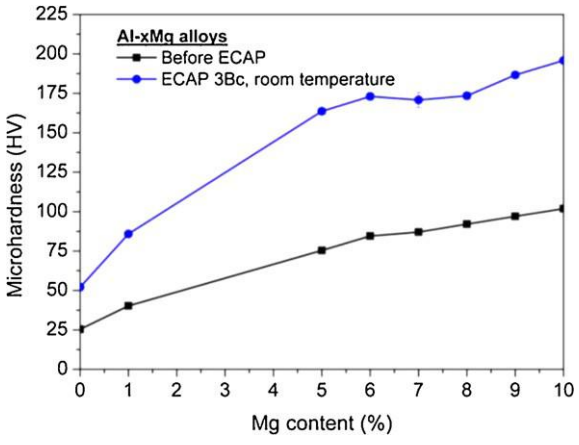

Fig. 6. Hardness changes in Al–xMg alloys before and after 3 ECAP passes at room temperature.

strength and improvement in ductility after 5 passes are caused by annealing after 4 passes, which is supposed to have obvious softening and to reduce the deformation defects. A good combination of both strength and ductility has been obtained at 6 passes, as shown in Fig. 8 and Table 2.

(4) Discussion

- Microstructural stability of Al–6 wt% Mg alloy

Hardness evolutions of Al–6 wt% Mg alloy after 6 passes of annealed ECAP are plotted against the annealing time in Fig. 9a. It is apparent that the hardness of the samples annealed at 473–623 K decreases sharply at the first 5 min and then reaches a plateau. Higher annealing temperature causes shorter time to reach lower hardness plateau. It is obvious that annealing at 573 K leads to a sharp decrease of the hardness plateau. Microstructure examinations on the annealed samples reveal that recovery plays an important role when annealing for 30 min at 523 K (seen in Fig. 9b) while full recrystallization has been finished in the samples annealed for 30 min at 573 K (seen in Fig. 9c). Therefore, the

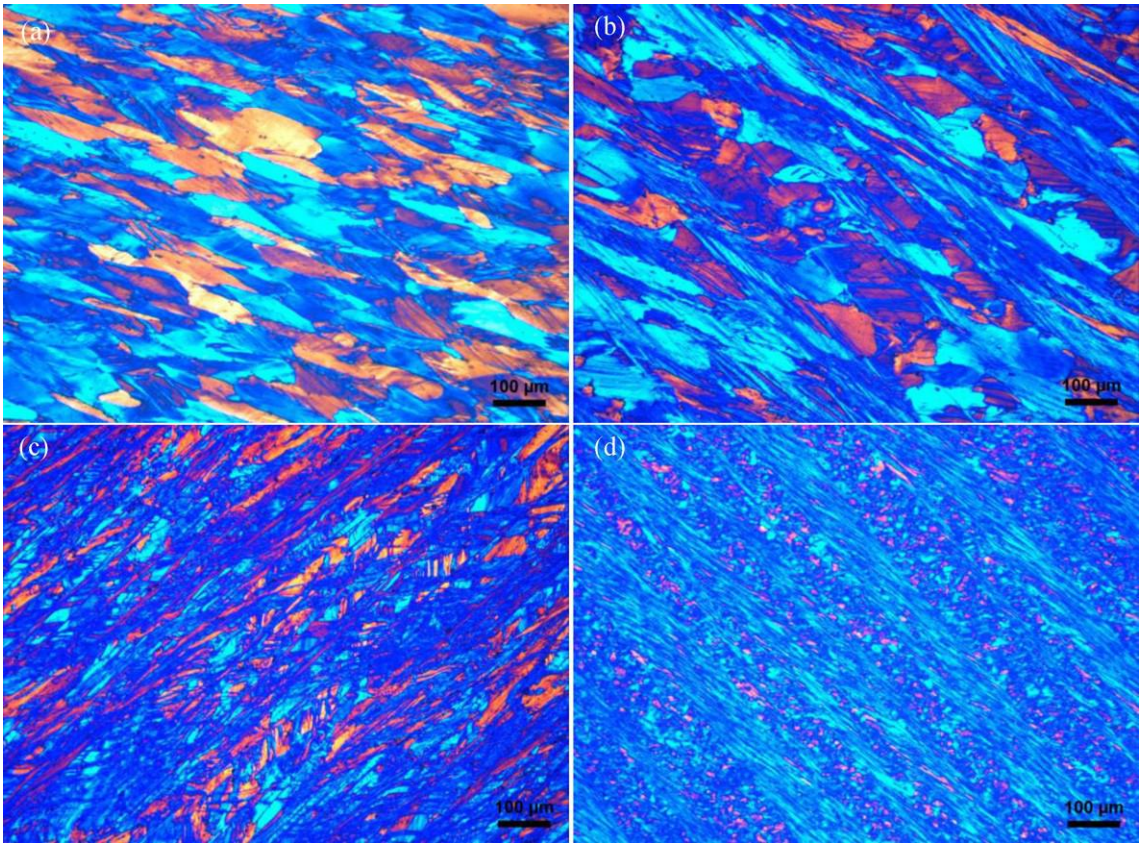

Fig. 7. Typical POM microstructures of Al–6 wt% Mg alloy processed by annealed ECAP at room temperature and passes of (a) 1, (b) 2, (c) 4 and (d) 6. Samples for 'annealed ECAP' were annealed at 523 K for 5 min and at 623 K for 10 min in an oven between the second and the third pass, and between the fourth and the fifth pass, respectively.

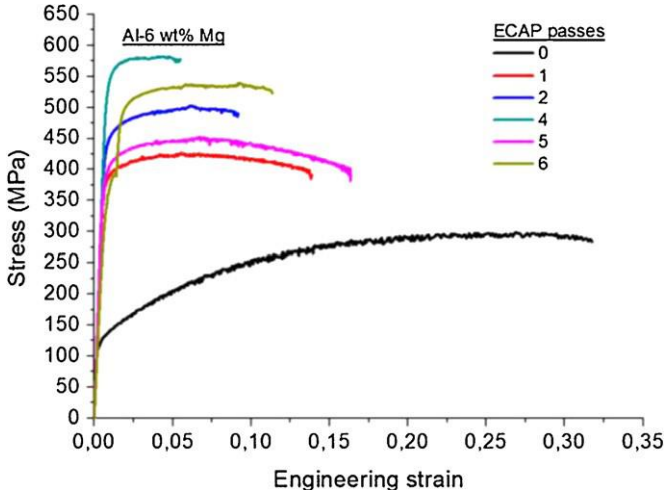

Fig. 8. Mechanical properties of Al–6 wt% Mg alloy processed by annealed ECAP.

change in softening mechanism of the Al–6 wt% Mg alloy, processed by 6 passes of annealed ECAP, occurs in the range of 523–573 K.

- Effect of Mg addition to aluminum

The addition of magnesium to aluminum increases the strength greatly (seen in Fig. 6) but it also makes the Al–xMg alloys less deformable. Before homogenization of these Al–xMg alloys, only Al–(0, 1 wt%) Mg alloys can be easily processed up to 4 ECAP passes at room temperature without any cracks. By contrast, small cracks have been found in the top surface of Al–10 wt% Mg alloy after the first pass of ECAP at 573 K. Very deep cracks have been observed after the second pass. Afterwards, homogenization has been considered to improve the deformability of all alloys. The homogenization greatly improves the deformability of Al–xMg alloys, especially for Al–xMg alloys containing high Mg content. However, the homogenized Al–(5–10 wt%) Mg alloys can only be deformed up to 3 passes at room temperature. In order to obtain higher ECAP strain at room temperature, short annealing on the strained samples is therefore employed. The strained Al–6 wt% Mg alloy with short annealing can be deformed successfully up to 6 passes.

Table 2
Summary of mechanical properties of Al–6 wt% Mg processed by annealed ECAP.

ECAP passes	Yield strength (YS, MPa)	Ultimate tensile strength (UTS, MPa)	Elongation (%)
0	127.4	296.6	3
1	401.5	426.3	1
2	472.7	503.2	9
4	562.2	582.5	5
5	425.6	453	1
6	–	539.4	1

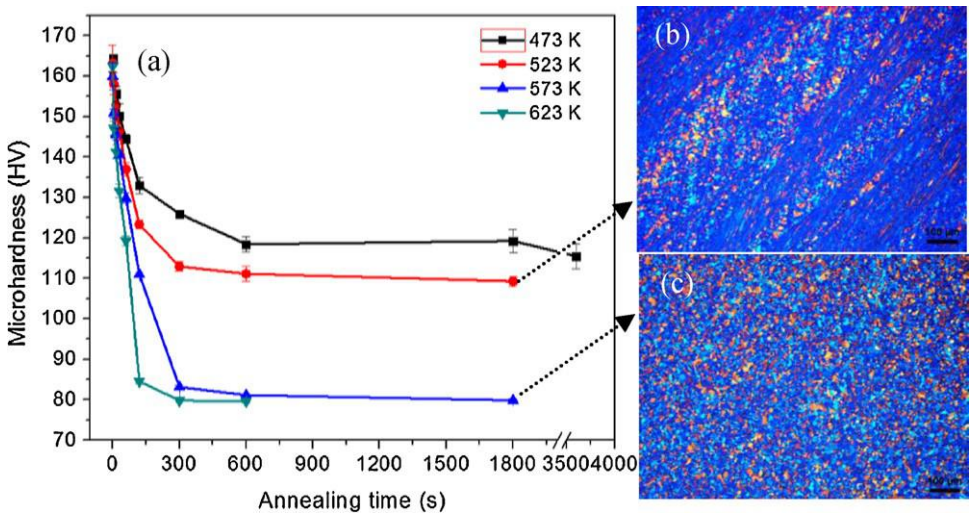

Fig. 9. (a) Hardness evolutions of Al–6 wt% Mg alloy after 6 passes of annealed ECAP as a function of annealing time, and the resulted microstructures after annealed for 30 min at (b) 523 K and (c) 573 K.

The results from this study show that the addition of magnesium to aluminum has significant influence not only on the deformation ability, but also on the microstructure and mechanical properties. It is well known that the addition of magnesium to aluminum lowers the stacking fault energy and leads to solid solution strengthening by reducing the dislocation mobility [13–15], which in turn leads to the decrease of minimum grain size in deformed Al–Mg alloys by increasing Mg content [13,14]. The results shown in Table 3 reveal that the fraction of HAGBs and the mean misorientation increase continuously with increasing magnesium content in Al–xMg alloys after ECAP. As a result, a smaller grain size is obtained in Al–xMg alloys containing higher Mg content. It should be noted that the mean grain size summarized in Table 3 always accompanies fine grains with grain size of 150–300 nm (shown in Fig. 5). In the ECAP processing of Al–xMg alloys, a large number of dislocations are introduced. It was reported that Mg addition up to 3 wt% dramatically increases the dislocation density in deformed Al–xMg alloys [15,16]. Therefore, higher dislocation density and lower rate of recovery in Al–xMg alloys can be obtained by increasing Mg content, which is thought to be the main reason for the increase

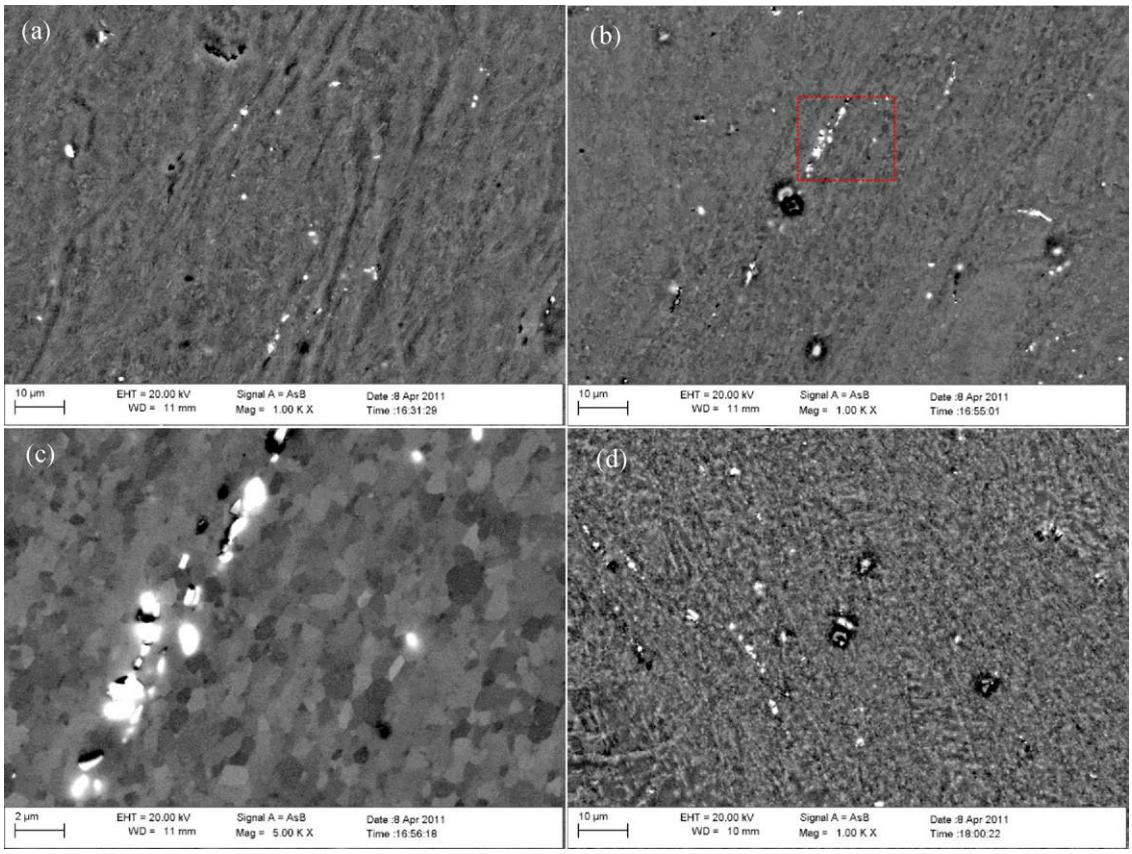

Fig. 10. Typical BSE microstructures of Al–xMg alloys processed by 3 ECAP passes showing the distribution of particles (a) Al–1 wt% Mg alloy, (b) and (c) Al–5 wt% Mg alloy at low and high magnification, respectively, (d) Al–7 wt% Mg alloy.

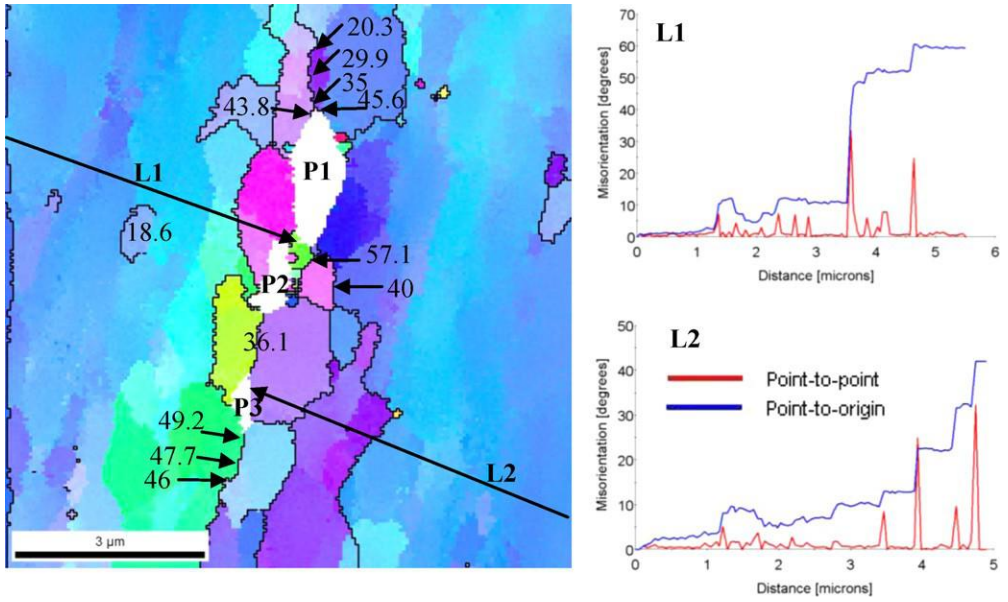

Fig. 11. A high resolution (step size 50 nm) EBSD map of a typical region around three particles (marked by P1–3) in Al–5 wt% Mg alloys, after 3 ECAP passes at room temperature, with HAGBs shown as thick black lines and the actual misorientations of selected HAGBs indicated in degrees.

in misorientation and the fraction of HAGBs, and the decrease of average grain size.

- Effect of particles

Fig. 10 presents the typical backscattered electron (BSE) microstructures of Al–xMg alloys processed by 3 ECAP passes. It can be seen that the number fraction of the particles is similar in the microstructures of Al–(1–10 wt%) Mg alloys because of their heat treatment history, as shown in Fig. 10a, b and d. The particles are bright due to atomic number contrast. The bright particles are iron rich particles and the size of the particles is around 1 μm. The particle distribution is relatively uniform in the matrix, although a weak tendency to distribute along the shear direction. It can be frequently observed that the particles are broken along the shear direction during ECAP (Fig. 10c).

Fig. 11 shows a high resolution EBSD map (step size 50 nm), of a typical region around three particles (marked by P1–3) in the Al–5 wt% Mg alloy, after 3 ECAP pass at room temperature. In this map, HAGBs are marked by thick black lines and two arrows are plotted (L1 and L2, perpendicular to the elongated direction) to examine how the orientation varies near the particles (the non-indexed white area in Fig. 11). Some misorientations of the selected HAGBs are indicated (in degrees). It can be seen that very high accumulated misorientations (point to origin) along L1 and L2 (42–59°) can be reached at a very short distance (~5 μm), indicating a very high misorientation gradient (up to 10.8°/μm) near the particles. It is 2.3 times the mean misorientation gradient of Al–1 wt% Mg alloy after 4 ECAP passes at cryogenic temperature [17]. Near the particles a deformation zone can be found where lots of fine grains/HAGBs generate, due to the influence of the particles. An important feature of the influence of the particles, which has never been published before, is a gradual misorientation increase along HAGBs close to particles. Examples of this feature have been indicated by the misorientation increase in one HAGB from 20.3° to 45.6°/43.8° and another one HAGB from 46° to 49.2°. Similar deformation zones have been observed around second-phase particles in Al alloys processed by ECAP [18]. It is well known that the effect of the second-phase particles on the microstructure during plastic deformation mainly depends on particle size [19,20]. This may be the reason why the larger particle stimulates higher misorientation (from 20.3° to 45.6°/43.8°) than the smaller one (seen in Fig. 11). Therefore, EBSD data reveals that the particles stimulate the misorientation increase along grain boundaries and the formation of fine grains/HAGBs.

Table 3
Summary of mean grain size, HAGBs% and mean misorientation in Al–xMg alloys after 3 ECAP passes obtained by EBSD data.

Alloys	HAGBs (%)	Mean grain size (nm)	Mean misorientation (°)
Pure Al	39	7	17.7
Al–5 wt% Mg	42.7	780	19
Al–7 wt% Mg	64.6	6	28.2
Al–10 wt%	65.7	5	28.8

(5) Conclusions

1. ECAP at room temperature results in considerable grain refinement of all Al–xMg alloys. The microstructures of Al–xMg alloys are refined by the interaction of shear bands and their increase in number.
2. The addition of magnesium to aluminum promotes the grain refinement.
3. Misorientation increase induced by particles along grain boundaries is observed by using high resolution EBSD.
4. As ECAP strain increases up to 4, the strength of Al–6 wt% Mg alloy increases progressively while the elongation decreases from 31.7% to 5.5%. A good combination of both strength and ductility has been obtained by annealed ECAP.
5. The change in softening mechanism of the Al–6 wt% Mg alloy, processed by 6 passes of annealed ECAP, occurs in the range of 523–573 K.

Acknowledgments

This work was supported by the Research Council of Norway under the Strategic University Program (192450/I30). We acknowledge Hydro Aluminum for providing samples and Mr. P.C. Skaret for performing ECAP processing and tensile testing.

References

[1] Y.C. Chen, Y.Y. Huang, C.P. Chang, P.W. Kao, Acta Mater. 51 (2003) 2005–2015.
[2] F. Dalla Torre, R. Lapovok, J. Sandlin, P.F. Thomson, C.H.J. Davies, E.V. Pereloma, Acta Mater. 52 (2004) 4819–4832.
[3] J. Wang, Y. Iwahashi, Z. Horita, M. Furukawa, M. Nemoto, R.Z. Valiev, T.G. Langdon, Acta Mater. 44 (1996) 2973–2982.
[4] R. Kapoor, J.K. Chakravartty, Acta Mater. 55 (2007) 5408–5418.
[5] Z. Horita, T. Fujinami, M. Nemoto, T.G. Langdon, Metall. Mater. Trans. 31A (2000) 691–701.
[6] B. Huarte, C.J. Luis, I. Puertas, J. Leon, R. Luri, J. Mater. Process. Technol. 162–163 (2005) 317–326.
[7] A. Vinogradov, A. Washikita, K. Kitagawa, V.I. Kopylov, Mater. Sci. Eng. A 349 (2003) 318–326.
[8] H.J. Roven, S. Dumoulin, J.C. Werenskiold, in: Y.T. Zhu, T.G. Langdon, R.Z. Valiev, S.L. Semiatin, D.H. Shin, T.C. Lowe (Eds.), Ultrafine Grained Materials III, TMS, Philadelphia, USA, 2004, pp. 117–124.
[9] Y.J. Chen, Y.J. Li, J.C. Walmsley, S. Dumoulin, S.S. Gireesh, S. Armada, P.C. Skaret, H.J. Roven, Scripta Mater. 64 (2011) 904–907.
[10] T.G. Langdon, Mater. Sci. Eng. A 462 (2007) 3–11.
[11] Y.J. Chen, J. Hjelen, S.S. Gireesh, H.J. Roven, J. Microsc. 245 (2012) 111–118.
[12] Y.T. Zhu, J.Y. Huang, J. Gubicza, T. Ungar, Y.M. Wang, E. Ma, R.Z. Valiev, J. Mater. Res. 18 (2003) 1908–1917.
[13] T. Morishige, T. Hirata, T. Uesugi, Y. Takigawa, M. Tsujikawa, K. Higashi, Scripta Mater. 64 (2011) 355–358.
[14] Y. Iwahashi, Z. Horita, M. Nemoto, T.G. Langdon, Metall. Mater. Trans. 29A (1998) 2503–2510.
[15] J. Gubicza, N.Q. Chinh, Z. Horita, T.G. Langdon, Mater. Sci. Eng. A 387–389 (2004) 55–59.
[16] J. Zhang, M.J. Starink, N. Gao, W. Zhou, Mater. Sci. Eng. A 528 (2011) 2093–2099.
[17] Y.J. Chen, H.J. Roven, S.S. Gireesh, P.C. Skaret, J. Hjelen, Mater. Lett. 65 (2011) 3472–3475.
[18] P.J. Apps, J.R. Bowen, P.B. Prangnell, Acta Mater. 51 (2003) 2811–2822.
[19] Q. Wang, Y. Chen, M. Liu, J. Lin, H.J. Roven, Mater. Sci. Eng. A 527 (2010) 2265–2273.
[20] C. Schafer, J. Song, G. Gottstein, Acta Mater. 57 (2009) 1026–1034.